Available online at www.sciencedirect.com
ScienceDirect
Journal of the European Ceramic Society 29 (2009) 711–716
www.elsevier.com/locate/jeurceramsoc

Shrinkage behavior of LTCC hetero-laminates

Won Bae Lim [a], Yong Soo Cho [a,*], Yong Jun Seo [a], Jae Gwan Park [b]

[a] *Department of Materials Science and Engineering, Yonsei University, Seoul 120-749, Republic of Korea*
[b] *Materials Science and Technology Division, Korea Institute of Science and Technology, Seoul 136-791, Republic of Korea*

Received 14 November 2007; received in revised form 20 July 2008; accepted 25 July 2008
Available online 14 September 2008

Abstract

Shrinkage behavior of various stacking configurations consisting of three dissimilar dielectric tapes with different dielectric constants of $k \sim 8.2$, 14.8 and 48.2 were investigated. The shrinkage behavior has been critical as a sensitive parameter in the design of embedded microcircuit passive components. Unexpectedly low *x–y* shrinkages of 2.5–7% observed for the hetero-configurations are believed to be associated with the physical constraining effect that results from the dissimilar sintering route and crystallization behavior of each tape. The constraining effect found depends on the sintering temperature and the total number of each tape layer in a given hetero-structure. The tendency of slope variation in the Arrhenius plots of thermo–mechanical curves suggests that increasing the number of embedded tapes can produce a potential lower activation energy with a higher *x–y* shrinkage.

Keywords: Ceramics; Glasses; Dielectric properties; LTCC

1. Introduction

Low temperature co-fired ceramics (LTCC) and related packaging technology have been extensively studied for the last decades due to their technical and industrial importance in various highly integrated and reliable components and packages.[1–6] This technology has not been restricted within the conventional ceramic packaging techniques, but has been extended to novel high dense packages incorporating various conductive and passive components.[7–10] One way to achieve dense packages may be the use of LTCC hetero-structures having different functionality.[11] There are various material parameters that need to be considered for the successful integration of the LTCC materials as overall performance. Physical constraining that comes from different densification routes may be one of the most important parameters when the reliability and reproducibility are critical.[12–15] Most of these reported studies on the so-called "constraining sintering" are based on LTCC materials designed to generate zero-shrinkage after firing.

This work reports the effects of different stacking ways of LTCC layers on the densification and crystallization of various symmetric laminated configurations consisting of three dissimilar LTCC tapes. The three tapes differ in their dielectric constant values, i.e., $k \sim 8.2$, $\sim$14.8, $\sim$48.2, respectively. The interest of the approach of incorporating different *k* tapes within a single component is related to the successful integration of embedded passives. These configurations may represent a good example of the potential combinations of low, middle, and high *k* LTCC tapes.

2. Experimental

Three LTCC tapes having different dielectric constants of 8.2, 14.8 and 48.2 were prepared for this work. These tapes were designated as Tape I, Tape II, and Tape III, respectively. The characteristics of three LTCC tapes are shown in Table 1. All these tapes were based on the mixture of glass and ceramic filler. Two types of selected glasses, which are based on calcium aluminoborosilicate (designated as G1) and barium titanium borate (G2), were produced by the typical glass melting/quenching process. Corresponding glass batches were melted in an uncovered platinum crucible by soaking at 1400 °C for G1 and 1500 °C for G2 for about an hour and then quenched into water to form clear

* Corresponding author. Tel.: +82 2 2123 7766; fax: +82 2 365 5882.
E-mail address: ycho@yonsei.ac.kr (Y.S. Cho).

0955-2219/$ – see front matter © 2008 Elsevier Ltd. All rights reserved.
doi:10.1016/j.jeurceramsoc.2008.07.058

Table 1
Basic characteristics of three LTCC tapes

ID	Glass code	Filler type	DTA data				Density (g cm^{-3})	k (1 MHz)	tanδ (1 MHz)
			T_g (°C)	T_s (°C)	1st $T_{c,onset}$ (°C)	1st $T_{c,peak}$ (°C)			
Tape I	G1	Al_2O_3	660	689	870	911	2.88	8.2	0.0004
Tape II	G2	Al_2O_3	640	661	760	793	3.46	14.8	0.0006
Tape III	G2	$BaTiO_3$	640	661	745	773	4.68	48.2	0.0010

glasses. The glasses were then ball-milled with stabilized zirconia balls for about 20 h, and dried on a hot plate while stirring by a magnetic bar.

As represented in Table 1, two kinds of filler powders as Al_2O_3 and $BaTiO_3$ were used. Al_2O_3 has been selected as a filler material as it is the most commonly reported filler in LTCC systems.[16–20] $BaTiO_3$ has been regarded as an easy choice for generating high dielectric constant since $BaTiO_3$ possesses high k of >3000.

For Tape I, the G1 glass was admixed with 34.2 vol.% of Al_2O_3 (99.9%, ALM-43, Sumitomo Chemical Co., Tokyo, Japan) filler. For Tape II and Tape III, the G2 glass was admixed with 52.8 vol.% Al_2O_3 and 23.1 vol.% $BaTiO_3$ (99.9%, Aldrich Chemical Co., Milwaukee, WI), respectively. A PVB-based organic binder (B-73225, Ferro Co., Cleveland, OH) system was used to make tape slurry by ball-mixing for about 6 h. The mixed slurry was cast on the Mylar-based film and dried in an oven at 120 °C for ~15 min. An average thickness of each dried tape was about 150 μm. Each layer of the dried tape was cut into a square form (2 in. × 2 in.), and then stacked onto a metal die before lamination.

Different stacking configurations using the three different tapes are illustrated in Fig. 1. Symbols of CONF-1 to CONF-6 represent the six configurations used in this study. All configurations are based on symmetrical arrays having low k tapes as outmost layers. Total number of individual layers was fixed as seven for all configurations and tapes for single composition (Tapes I–III). The number of individual tape layer in each configuration is shown in Table 2. All configurations were laminated and then sintered at a peak temperature of 850 °C for 30 min, at a heating rate of 5 °C/min.

X–y shrinkage was measured for the fired samples by comparing sample dimensions in the x–y plane before and after firing.

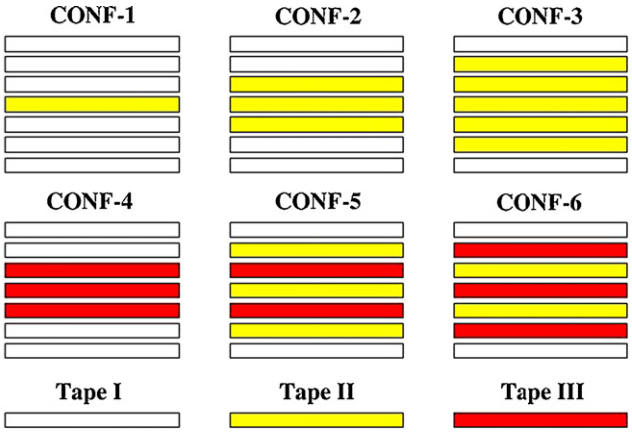

Fig. 1. Configuration schematic of various LTCC hetero-structures.

Dielectric properties of fired tape samples were measured at 1 MHz by an impedance analyzer (HP 4194A, Hewlett Packard, Palo Alto. CA). The fired tape samples were electroded with a Ag paste prior to the dielectric measurement. Firing behavior was determined by a differential thermal analyzer (TG/DTA-92, SETRAM Co., Calurie, France) at a fixed heating rate of 5 °C/min. The powder mixture of each tape composition was used for the DTA runs. Dimensional change in z direction, which corresponds to thickness variation of the laminates, was recorded at a heating rate of 5 °C/min, by thermo–mechanical analysis (TMA) using a dilatometer (Dilatonic Tokyo Industry, Japan). The sample of 1 cm × 1 cm × 0.07 cm was used for the TMA measurement. The cross-sections of the sintered samples were examined by scanning electron microscopy (XL-30 ESEM, FEI-Philips, Netherlands).

Table 2
Values of x–y shrinkage and apparent activation energy for densification in various LTCC hetero-structures

ID	The number of consisting tapes			Measured x–y shrinkage (%)	E_a[a] (kJ mol^{-1})
	Tape I	Tape II	Tape III		
Tape I	7	–	–	16.4	439
Tape II	–	7	–	11.2	833
Tape III	–	–	7	14.1	618
CONF-1	6	1	–	4.4	751
CONF-2	4	3	–	5.2	537
CONF-3	2	5	–	7	518
CONF-4	4	–	3	2.5	454
CONF-5	2	3	2	5.5	669
CONF-6	2	2	3	5.3	609

[a] The E_a values were averaged over the multiple trials and selected within the error range of ±5%.

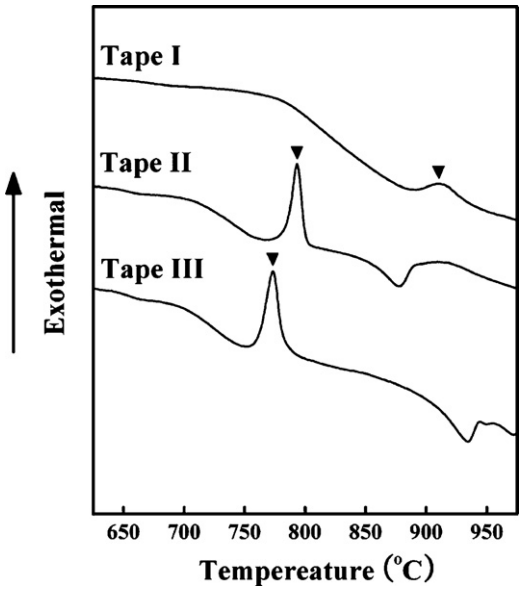

Fig. 2. DTA curves of Tapes I–III.

3. Results

Some important physical and dielectric properties of the LTCC Tapes I–III used in this study are shown in Table 1. The glass characteristics, such as glass transition point (T_g) and softening point (T_s), were obtained from the DTA curve (Fig. 2). The G1 glass appeared to have slight higher T_g and T_s compared to the G2 glass. The peak crystallization temperature ($T_{c,\,peak}$) of Tape I was 911 °C as seen in the exothermal peak of Fig. 2. The first crystallization temperatures of Tapes II and III containing the same glass G2 were different as 793 and 773 °C, respectively. It suggests that crystallization of the G2 glass depends on the type of filler and, subsequently, occurs likely from certain chemical reactions between the glass and filler.[19,20] Other parameters such as fired density and dielectric properties, measured for the samples fired at 850 °C for 30 min, are also represented in Table 1.

Fired tapes of various configurations did not show any warps or cracks, which may affect absolute values of fired shrinkage. Fig. 3 shows the cross-sectional example of backscattered SEM image corresponding to CONF-6. Each tape layer can be easily distinguished as being matched well with the original stacking sequence (Fig. 3(a)). The enlarged cross-section seen in Fig. 3(b) represents two interface regions; one between Tape I and Tape III and the other between Tape III and Tape II. There were no cracks throughout the interfaces.

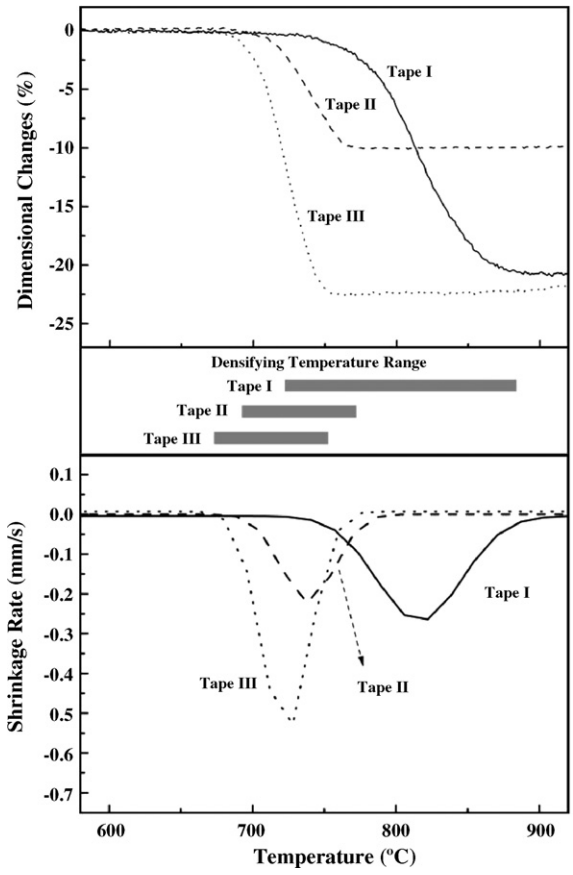

Fig. 4. Shrinkage behavior of Tapes I–III, obtained by the TMA measurement.

The fired *x*–*y* shrinkage values of all tapes and configurations fired at 850 °C are represented in Table 2. The three tapes I–III showed shrinkages of 16.4, 11.2 and 14.1%, respectively. In the case of different configurations, overall *x*–*y* shrinkage was found to vary depending on the relative number (or the relative thickness) of individual tape layer in the given configuration. There is an increasing tendency for *x*–*y* shrinkage with increasing the number of Tape II layer in the configurations of the two dissimilar tapes (Tapes I and II) as illustrated in the CONF-1–3. For example, shrinkage increased from 4.4 to 7% by increasing the number of Tape II layer from one to five (CONF-1 to CONF-3).

Fig. 4 shows the changes in the *z* shrinkage (or sample thickness). The densification behavior of the three LTCC tapes

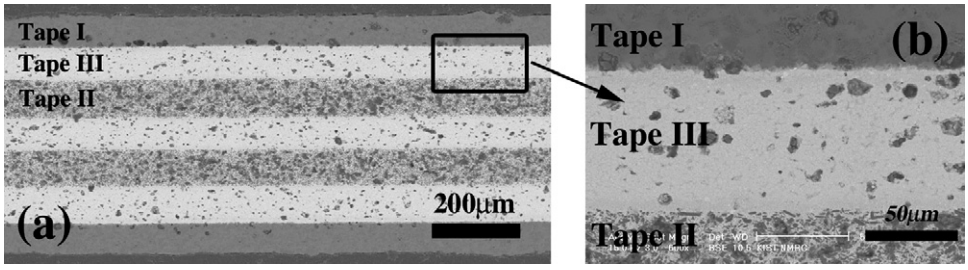

Fig. 3. Backscattered SEM images of the CONF-6 cross-section.

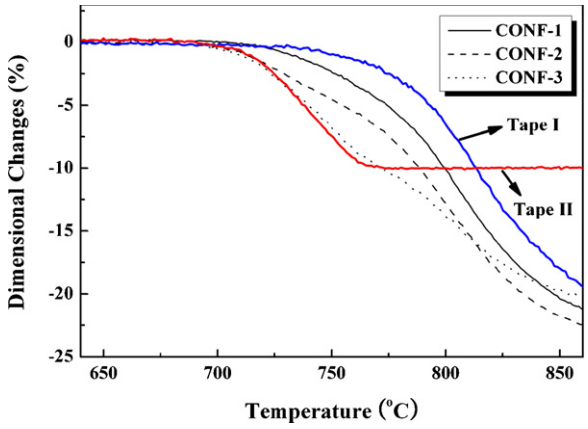

Fig. 5. TMA curves of LTCC hetero-structures consisting of Tapes I and II.

differs significantly. The temperature ranges of initial sintering were carefully determined by collecting the data within 3% of shrinkage for each sample.[22–24] Densification of Tape I starts at a higher temperature (~720 °C) when compared to Tape II (~690 °C) or Tape III (~670 °C). In addition, the densification of Tape I appeared to be more sluggish as the dimensional change happens over a broader temperature range of 720–885 °C. Densifications of Tape II and III occur more rapidly within a relatively short temperature range of 690–770 °C for Tape II and 670–755 °C for Tape III.

Figs. 5 and 6 show the additional TMA curves of selected configurations to illustrate the firing behavior of the LTCC hetero-structures and to correlate their behavior with that of individual tapes. Fig. 5 represents TMA curves of configurations (CONFs-1 and 3) consisting of Tapes I and II. As expected, the z shrinkage behavior of these configurations tended to follow the mixed route between individual densification curves of Tapes I and II in Fig. 4. For example, the dimensional curve of CONF-2 was located in the region formed between the curves of Tapes I and II. The densification curve tended to shift to lower temperatures as increase in the number of Tape II.

Fig. 6 shows the TMA curves for the CONFs-5 and 6 consisting of all the three Tapes I, II and III. The z shrinkage behavior

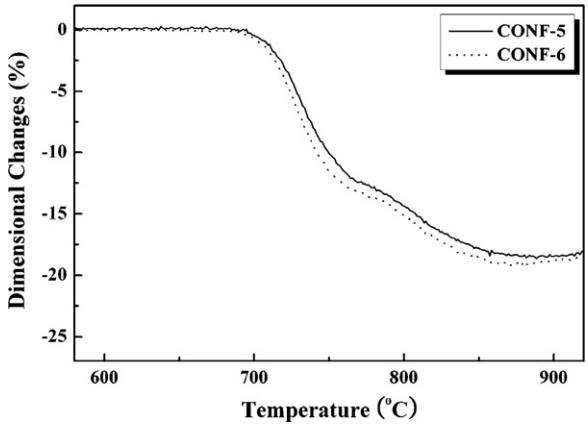

Fig. 6. TMA curves of LTCC hetero-structures consisting of three dissimilar tapes.

changed depending on the densification route of each tape and also the number of each tape layer. The CONF-6 with more number of Tape III layers (three layers for CONF-6 vs. two layers for CONF-5) showed a lowered densification route, which is closer to the behavior of Tape III.

4. Discussion

Densification behavior in Fig. 4, which can be characterized with onset and ending densification temperature and densification kinetics, seems to be associated with the softening and crystallization temperatures represented in Table 1. Softening point of glass must determine the starting point of densification since glass is the source of the low temperature sintering. Densification in Tapes II and III starts earlier than in Tape I (Fig. 4) because the G2 glass has a lower softening point of 661 °C than the G1 glass with $T_s \sim 689$ °C.

On the other hand, the ending point of densification curves in Fig. 4 matches well with crystallization temperature of each tape (Table 1). For example, the curve of Tape II in Fig. 4 ended at ~760 °C, which is the onset temperature of the first crystallization peak in the DTA curve of Fig. 2. Similarly, densification of the other two Tapes I and III stopped around the onset temperature of crystallization 870 and 745 °C, respectively (Table 1). Densification is unlikely to proceed further once crystallization starts to occur and subsequently the relative amount of low viscosity glass is dramatically reduced. It is suggested as an ideal case where full densification is achieved prior to crystallization.

The measured x–y shrinkage values of 2.5–7% in hetero-configurations are substantially lower than the shrinkage values of individual Tape I, II, and III. The x–y shrinkage values of Tapes I–III are 16.4, 11.2 and 14.1%, respectively as represented in Table 2. The decrease in shrinkage and their dependence on the number of each layer is likely to be associated with the difference in densification routes and kinetics as seen in Fig. 4. The difference induces physical constraining effect of each tape during densification upon firing. Tape having a slower densification rate must determine overall densification behavior of the given hetero-configuration by retarding dimensional movement of tape with a higher densification rate.

The constraining effect depends on specific temperature region defined by the sintering attributes of each tape in the hetero-structures. In the case of CONF-1–3 consisting of Tapes I and II, for instance, overall x–y shrinkage is likely to be controlled by Tape I up to 770 °C since the densification of Tape I occurs more slowly up to that temperature (Fig. 4). In the region above 770 °C where the sintering of Tape II almost stops, Tape II controls the overall shrinkage. Accordingly, Fig. 7 represents the dominant regions of the constraining effect by each tape in the hetero-configuration cases containing either Tape II or Tape III as embedded layers. In any case, Tape I controls shrinkage behavior of the hetero-structure up to the point where Tape II or Tape III starts crystallization. Higher values of x–y shrinkage obtained with more number of Tape II layers in CONF-1 –3 suggests that the degree of constraining effect by Tape I in the early temperature region becomes less as the number of Tape II

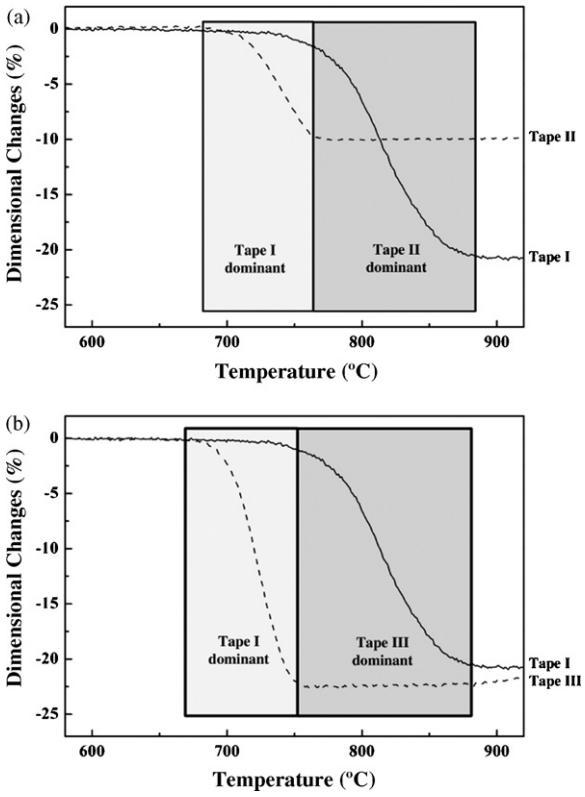

Fig. 7. Schematic of the physical constraining regions in TMA curves.

increases. The larger relative volume (or thickness) of a tape in hetero-structures is likely to create the stronger effect towards the intrinsic behavior of the tape.

Similarly, in the case of Tapes I–III configurations, Tape I is believed to control dominantly the shrinkage behavior up to ~755 °C, where the densification of Tape III stops due to its crystallization (Fig. 7(b)).

From TMA curves of the hetero-configurations, densification behavior of various LTCC configurations was further studied by using an Arrhenius equation:

$$\frac{\Delta L/L_0}{T} = \text{const} \cdot \exp\left(\frac{-mE_a}{RT}\right) \quad (1)$$

where $\Delta L/L_0$ is the linear z shrinkage, E_a is the apparent activation energy for densification, T is the temperature, and R is the gas constant.[21–23] The constant m is given depending on sintering mechanism. Taking the logarithm in both sides of Eq. (1) results in

$$\ln\left(\frac{\Delta L/L_0}{T}\right) = \frac{-mE_a}{RT} + \text{const} \quad (2)$$

Fig. 8 shows the plots of $\ln[(\Delta L/L_0)/T]$ vs. $1/T$, which were obtained in the temperature range corresponding to the initial sintering stage of each configuration in the TMA curves of Figs. 4–6. The slope of each plot indicates the apparent activation energy for densification. Table 2 shows the calculated apparent activation energy for densification of each configuration. These calculated energies are based on the reasonable assumption ($m = 1$) that the sintering mechanism is predominantly viscous

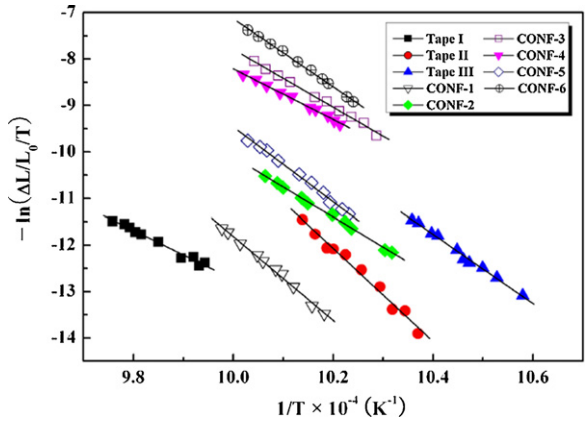

Fig. 8. Arrhenius plots of $\ln[(\Delta L/L_0)/T]$ vs. $1/T$.

flow. The slope of Tape II showed a highest negative value, suggesting that higher activation energy is required for densification of Tape II compared to other LTCC configurations. Increasing the number of Tape II in a given hetero-structure (see CONF-1–3 and CONF-5 and 6) tends to gradually reduce absolute values of the slopes and thus requires lower activation energies for densification. For example, apparent activation energy of 518 kJ/mol was obtained for the CONF-3 (having five Tape II layers) compared to 751 kJ/mol CONF-1 (having one Tape II layer). Overall, higher values of x–y shrinkage are found to be associated with less activation energies while understanding the absolute number of the energy seems to be complicated with the type and densification kinetics of given tapes.

5. Conclusions

Fired x–y shrinkage values depended on the relative number of individual tape layers in a given LTCC configuration, consisting of three dissimilar LTCC tapes having different dielectric constant $k \sim 8.2$, 14.8 and 48.2. The shrinkage dependence is believed to be associated with the physical constraining effect of each tape during densification. It is assumed that Tape I with a slower densification rate determines dominantly overall x–y shrinkage of the LTCC hetero-structures particularly below the crystallization temperature of either Tape II or III. The constraining effect driven by dissimilar densification routes and subsequent crystallization was understood as the major reason for the observed lower x–y shrinkage of 4.4–7% for the hetero-configurations. Calculated apparent activation energies for densification suggest that the required energy level depends on the type and, consequently, the shrinkage behavior of a given hetero-laminate.

Acknowledgement

This research was supported by a grant funded by the Ministry of Commerce Industry and Energy (MOCIE), Republic of Korea.

References

1. Cho, Y. S. and Yoon, K. H., *Handbook of Advanced Electronic and Photonic Materials and Devices*. Academic Press, San Diego, 2001, pp. 175–199.
2. Cho, Y. S., Hang, K. W., Barker, M. F., Ollivier, P., Wang, C. B., Amey, D. I. *et al.*, New Pb free tape system for automotive and telecommunication applications. In *Proceddings of the IMAPS Ceramic Interconnect Technology Conference*, 2004, pp. 226–230.
3. Cho, Y. S., Hang, K. W., Wang, C. B., Souders, K. E., Majumdar, D., Amey, D. *et al.*, High k LTCC system for high frequency applications. In *Proceedings of the IMAPS Ceramic Interconnect Technology Conference*, 2003, pp. 195–199.
4. Saito, K., Murase, H., Utaki, H. and Yamamoto, T., Tunable active filters having multilayer stucture using LTCC. *IEEE. Trans. MTTS.*, 2001, **49**, 2421–2424.
5. Kim, S. H., Yim, J. H. and Kim, B. M., A new planar-type dielectric resonatro using LTCC technology for mm-wave band applications. *Microw. Opt. Technol. Lett.*, 2005, **44**, 533–536.
6. Yeung, L. K., Wang, J., Huang, Y., Lee, S. C. and Wu, K. L., Acompact LTCC bluetooth system module with an integrated antenna. *Int. J RF. Microw. Comput-Aid. Eng.*, 2006, **16**, 238–244.
7. Steinverg, J. I., Horowitz, S. J. and Bacher, R. J., Low temperature co-fired tape dielectric material systems for multilayer interconnections. In *Advances in Ceramics, Westerville*, ed. J. B. Blum and W. R. Cannon, 1986, p. 31.
8. Niwa, K., Namehara, K., Yokoyama, H. and Kurihara, K., Multilayer ceramic circuit board with copper conductors. In *Advances in Ceramics, Westerville*, ed. J. B. Blum and W. R. Cannon, 1986, p. 41.
9. Shimada, Y., Utsumi, K., Suzuki, M., Takamizawa, H., Nitta, M. and Watari, T., Low firing temperature multilayer glass–ceramic substrate. *IEEE. Trans. Comp. Hybrids Manuf. Techol.*, 1983, **6**, 382–388.
10. Rusu, C., Persson, K., Ottosson, B. and Billger, D., LTCC interconnects in microsystems. *J Micromech. Microeng.*, 2006, **16**, S13–S18.
11. Modes, C., Malkmus, S. and Gora, F., High K low loss dielectrics co-fireable with LTCC. *Active Passive Elec. Comp.*, 2002, **25**, 141–145.
12. Lin, Y. C. and Jean, J. H., Constrained densification kinetics of alumina/borosilicate glass + alumina/alumina sandwich structure. *J. Am. Ceram. Soc.*, 2002, **85**, 150–154.
13. Lei, C. D. and Jean, J. H., Effect of crystallization on the stress required for constrained sintering of $CaO–B_2O_3–SiO_2$ glass–ceramics. *J. Am. Ceram. Soc.*, 2005, **88**, 599–603.
14. Mohanram, A., Lee, S. H., Messing, G. L. and Green, D. J., Constrained sintering of low-temperature co-fired ceramics. *J. Am. Ceram. Soc.*, 2006, **89**, 1923–1929.
15. Mohanram, A., Messing, G. L. and Green, D. J., Densification and sintering viscosity of low-temperature co-fired ceramics. *J. Am. Ceram. Soc.*, 2005, **88**, 2681–2689.
16. Choi, Y. J., Park, J. H., Ko, W. J., Hwang, I. S., Park, J. H. and Park, J. G., Co-firing and shrinkage matching in low- and middle-permittivity dielectric compositions for a low-temperature co-fired ceramics system. *J. Am. Ceram. Soc.*, 2006, **89**, 562–567.
17. Dai, S. X., Huang, R. F. and Wilcox Sr., D. K., Use of titanates to achieve a temperature-stable low-temperature cofired ceramic dielectric for wireless applications. *J. Am. Ceram. Soc.*, 2002, **85**, 828–832.
18. Jean, J. H., Chang, C. R., Chang, R. L. and Kuan, T. H., Effect of alumina particle size on prevention of crystal growth in low-k silica dielectric composite. *Mater. Chem. Phys.*, 1995, **40**, 50–55.
19. Chen, C. L., Wei, W. C. J. and Roosen, A., Wetting, densification and phase transformation of $La_2O_3/A_2O_3/B_2O_3$-based glass–ceramics. *J. Eur. Ceram. Soc.*, 2006, **26**, 59–65.
20. Seo, Y. J., Shin, D. J. and Cho, Y. S., Phase evolution and microwave dielectric properties of lanthanum borate-based low-temperature co-fired ceramics materials. *J. Am. Ceram. Soc.*, 2006, **89**, 2352–2355.
21. Theunissen, G. S. A. M., Winnubst, A. J. A. and Burggraaf, A. J., Sintering kinetics and microstructure development of nanoscale Y-TZP ceramics. *J. Eur. Ceram. Soc.*, 1993, **11**, 315–324.
22. Young, W. S. and Cutler, I. B., Initial sintering with constant rates of heating. *J. Am. Ceram. Soc.*, 1970, **53**, 659–663.
23. Pérez-Maqueda, L. A., Criado, J. M. and Real, C., Kinetics of the initial stage of sintering from shrinkage date: simultaneous determination of activation energy and kinetic model from a single nonisothermal experiment. *J. Am. Ceram. Soc.*, 2002, **85**, 763–768.
24. German, R. M., *Sintering Theory and Practice*. John Wiley and Sons, Inc, New York, 1996, pp. 98–103.